Submitted to

International Europhysics Conference on High Energy Physics, EPS03, July 17-23, 2003, Aachen
(Abstract **084** Parallel Session **4**)

XXI International Symposium on Lepton and Photon Interactions, LP03, August 11-16, 2003, Fermilab

www-h1.desy.de/h1/www/publications/conf/conf_list.html

Measurement of the Proton Structure Function F_2 at low Q^2 in QED Compton Scattering at HERA

H1 Collaboration

Abstract

The proton structure function F_2 is measured in QED Compton scattering at HERA using data collected in 1997 by the H1 experiment. QED Compton events give access to the kinematic range of very low Q^2, down to $0.1\ \mathrm{GeV}^2$, and medium Bjorken x, a region which is not covered by inclusive DIS measurements at HERA. The results are in agreement with the measurements from fixed target experiments wherever they overlap.

1 Introduction

Measurements of deep-inelastic lepton-proton scattering (DIS) provide information that is crucial to our understanding of proton structure. Since the fixed target experiments have discovered scaling violations [1,2], much progress has been made in extending the kinematic range of measurement in terms of the Bjorken variable x and the four-momentum transfer Q^2. Especially the HERA ep scattering experiments have shown that the Q^2 evolution of the proton structure function $F_2(x, Q^2)$ is well described by perturbative Quantum Chromodynamics (pQCD) throughout a wide range in x and Q^2 [3–6]. However, at small Q^2 deviations from pQCD predictions are observed [6, 7], indicating the transition into a regime in which non-perturbative effects dominate and the data can only be described by phenomenological models such as those derived from the Regge approach [8].

In order to study this non-perturbative regime, the structure function F_2 has been measured at very low values of Q^2 and x, which are accessible at HERA via special devices mounted close to the outgoing electron beam direction [7] thus facilitating measurements of the scattered electron at very low angles. These devices, however, do not cover the transition region at $Q^2 \sim 1\,\mathrm{GeV}^2$, which up to now has only been investigated using “shifted vertex” data [9, 10]. In this paper preliminary results of a new measurement of F_2 in this kinematic domain are presented, which utilises ep data with wide angle hard photon radiation, so called QED Compton (QEDC) events.

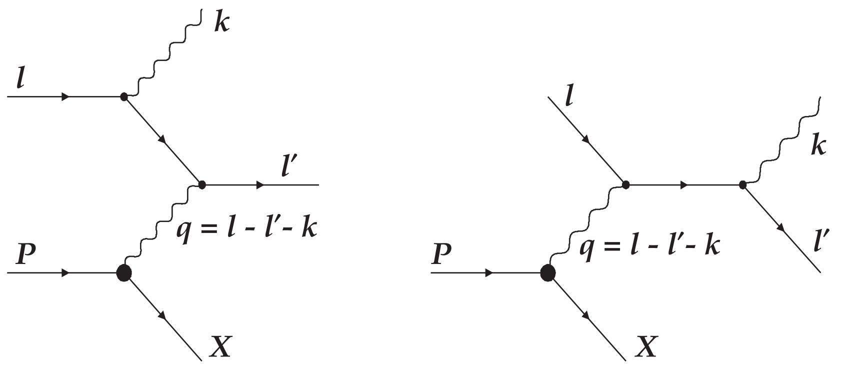

Figure 1: Lowest order Feynman diagrams for the radiative process $ep \to e\gamma X$ with photon emission from the electron line. l, P represent the four-momenta of the incoming electron and the incoming proton, while l', k and X are the momenta of the scattered electron, the radiated photon and the hadronic final state, respectively.

2 QED Compton Scattering Cross Section

Radiative processes in ep scattering, as depicted in fig. 1, may be split into three different classes [11, 12] with (i) the bremsstrahlung or Bethe-Heitler process corresponding to small masses of both the virtual electron and the virtual photon, (ii) the QED Compton process with a low virtual photon and a large virtual electron mass and finally (iii) the radiative DIS process where the photon is collinear either with the incoming (Initial State Radiation, ISR) or the outgoing (Final State Radiation, FSR) electron. All three classes correspond to distinct experimental signatures. For the QEDC scattering process the final state topology is given by an azimuthal back-to-back configuration of the outgoing electron and photon detected under rather large scattering angles. In this configuration their transverse momenta balance such that very low values of the exchanged photon virtuality Q^2 are experimentally accessible.

To correctly describe the process $ep \to e\gamma X$ the standard kinematic variables x and Q^2, used to describe inclusive deep-inelastic scattering (DIS), have to be redefined in order to account for the additional photon in the final state

$$Q^2 = -q^2 = -(l - l' - k)^2 \ , \quad x = \frac{Q^2}{2P \cdot (l - l' - k)} \ , \quad y = \frac{Q^2}{xs} \ . \tag{1}$$

Here l and P are the four-momenta of the incoming electron and the incoming proton, and l' and k represent the momenta of the scattered electron and the radiated photon, respectively (fig. 1). Three further independent variables are needed for a full description of the differential QEDC scattering cross section. In the formalism presented in [11] the Lorentz invariant scale variable $x_\gamma = q \cdot l / P \cdot l$ and the scattering solid angle Ω^* defined in the centre-of-mass frame of the virtual Compton process are employed. The cross section is then given by [11]

$$\frac{d^4\sigma^{ep \to e\gamma X}}{dx dx_\gamma dQ^2 d\Omega^*} = f^T_{\gamma^*/p}(x, x_\gamma, Q^2) \left[\frac{d\sigma}{d\Omega^*}\right]^T + f^L_{\gamma^*/p}(x, x_\gamma, Q^2) \left[\frac{d\sigma}{d\Omega^*}\right]^L \ , \tag{2}$$

where $[d\sigma/d\Omega^*]^{T,L}$ are the differential cross sections of the process $e\gamma^* \to e\gamma$ for transverse and longitudinal polarised photons, fully calculable in the framework of QED [11], and $f^{T,L}_{\gamma^*/p}$ represent the corresponding virtual photon spectra, which may be expressed in terms of the photo-absorption cross sections $\sigma^{T,L}_{\gamma^* p}$. In order to specify $\sigma^{T,L}_{\gamma^* p}$ one has to consider three separate contributions depending on the value of the invariant mass W of the outgoing hadronic final state:

1. Elastic scattering, for which the proton stays intact ($W = m_p$). This channel is well measured, and the cross section is given by the electric and magnetic form factors G_E and G_M;
2. Resonance production, where the total mass of the hadronic final state X lies in the range $m_p + m_\pi \lesssim W \lesssim 2\,\mathrm{GeV}$;
3. Continuum inelastic scattering at $W \gtrsim 2\,\mathrm{GeV}$. In this region the $\gamma^* p$ cross section is defined through the proton structure functions F_2 and F_L.

The above cross section expression (2) is implemented in the COMPTON Monte Carlo event generator [13]. The program also calculates higher order corrections for Initial State Radiation in the peaking approximation [14, 15]. However, as this generator was primarily written for an application in analyses of elastic QEDC events, in the original version a rather basic approach is employed to describe the resonance region and only simple scale invariant F_2 parameterisations are used to model the continuum inelastic domain. Furthermore, no hadronisation of the final state X is performed.

Since this analysis aims at the investigation of inelastic QEDC events a new version of the COMPTON generator was developed [16] which includes detailed parameterisations for the resonance [17] and the continuum [18] regions. In addition, several packages for a complete simulation of the hadronic final state have been implemented into the program. For the present study the SOPHIA package [19] is used in the range of low Q^2 and low masses, W, of the hadronic final state, while the Quark Parton Model with subsequent Lund string fragmentation [20] is employed at high W and high Q^2.

The SOPHIA model which is employed in most of the analysed phase space provides a minimum bias description of photoproduction processes reproducing a large set of available data. To be specific, the production of major baryon resonances, direct pion production, multiparticle production based on the Dual Parton Model [21] with subsequent Lund string fragmentation, as well as the diffractive production of light vector mesons ρ and ω are simulated.

3 Experimental Technique

The outgoing electron and photon in QEDC events are selected in the H1 detector [22] by requiring two energy depositions (clusters) in the electromagnetic part of the backward[1] lead-fibre calorimeter SpaCal [23] with a polar acceptance of $153° < \theta < 177°$, an electromagnetic energy resolution of $\sigma/E = 7\%/\sqrt{E/\mathrm{GeV}} \oplus 1\%$ and the spatial resolution of $\sigma = 6.3\,\mathrm{mm}/\sqrt{E/\mathrm{GeV}} \oplus 1.7\,\mathrm{mm}$. The Backward Drift Chamber (BDC) [24] situated in front of the SpaCal and providing an average resolution of 0.57 mrad for the θ measurement is employed as a pre-shower detector to increase the precision of the cluster position measurement for electrons and converted photons. In events with the electron scattered in the inner part of the SpaCal, the Backward Silicon Tracker (BST) [25] with an angular coverage of $171.5° < \theta < 176.5°$ and resolution of 0.3 mrad is used to measure the electron polar angle and to reconstruct the interaction vertex position. In events in which the electron is scattered out of the BST acceptance, the Central Inner Proportional Chamber (CIP) [22] in conjunction with BDC and SpaCal is employed to determine the vertex coordinates. The vertex reconstruction efficiencies are measured using inclusive DIS data and found to be 91% on average for the BST and above 99% for the CIP. The hadronic final state is measured in the Liquid Argon Calorimeter (LAr) [22] covering the angular range $4° < \theta < 153°$. It has an energy resolution of $12\%/\sqrt{E} \oplus 1\%$ for the electromagnetic and $50\%/\sqrt{E} \oplus 2\%$ for the hadronic section.

The analysed events were collected using a dedicated QEDC trigger chain ivolving three trigger levels. The chain is designed to select events with two clusters in the electromagnetic SpaCal with the azimuthal back-to-back topology. Unfortunately, this trigger chain was built to keep only elastic QEDC events, which are extensively used for detector alignment, calibration and luminosity cross checks. A significant number of events with hadronic activity in the central

[1]The z axis of the right-handed coordinate system used by H1 is defined to lie along the direction of the incident proton beam and the origin to be at the nominal ep interaction vertex. The backward direction is thus defined through $z < 0$.

region of the detector were rejected by additional conditions based on the tracks in the Central Jet Chamber. The phase space of the measurement is therefore restricted to the range where the hadronic final state is detected in the forward part of the detector. The trigger efficiency is determined as a function of the largest polar angle θ_{LAr} of a cluster in the LAr calorimeter with the energy above the noise threshold of 0.5 GeV and falls down from 99% at minimum θ_{LAr} to 79% at $\theta_{\mathrm{LAr}} = 30°$. The efficiencies of all other trigger conditions are $\gtrsim 99\%$.

4 Background Processes

A prominent background to inelastic QEDC scattering is created by inclusive DIS events in which one particle from the hadronic final state (typically a π^0) fakes the outgoing photon producing a cluster in the electromagnetic SpaCal. At high y, where the hadronic final state lies mostly in the hemisphere of the scattered electron and photon, this process dominates the QEDC signal making a clear QEDC event selection impossible. For this reason the measurement is restricted to relatively low y values: $y \lesssim 0.006$. Inclusive DIS events are modelled using the DJANGO MC generator [26] which includes LEPTO [27] and ARIADNE [28] for the hard interaction and higher order QCD effects as well as HERACLES [29] for the calculation of leading order radiative corrections. DJANGO events with hard photons emitted from the lepton side in the analysed phase space are excluded from the analysis to avoid double counting with COMPTON events. It however cannot be a priori expected that the specific non-perturbative process of single π^0 production far from the other final state hadrons is correctly simulated by an inclusive event generator. The DIS background sample is therefore renormalised after extensive dedicated studies, which resulted into scaling down the DJANGO contribution by a factor of 1.8. The DIS background is thus estimated to contribute up to 3% of the total cross section with a systematic uncertainty of 100%.

Another source of significant background is Deeply Virtual Compton Scattering (DVCS), in which the final state photon is radiated from the proton side. DVCS and QEDC are indistinguishable experimentally, and differ only in the kinematic distributions of the outgoing electron and photon. The interference between the two processes does not influence the energy and polar angle distributions of the final state particles in the leading twist approximation, thus allowing for separate MC simulations of both processes. Elastic DVCS events were simulated by the TINTIN generator [30] and the cross section was normalised to the H1 results [31].

At present there is no theoretical prediction and no measurement for the inelastic DVCS cross section. The ratio of the inelastic to elastic scattering cross section was therefore estimated experimentally to be of a similar size as for diffractive vector meson electroproduction. From this inelastic DVCS is derived to contribute 5.5% of the measured cross section with a 100% uncertainty.

Further background sources considered are typically of the order $\lesssim 1\%$. These are:

- elastic and inelastic dilepton production, modelled using the GRAPE event generator [32].
- inclusive photoproduction, simulated by the PHOJET program [33] which in particular includes production of light vector meson ρ, ω and ϕ;

- diffractive electroproduction of light vector mesons as well as diffractive J/ψ photo- and electroproduction, all being simulated by the DIFFVM MC generator [34] for both elastic and proton-dissociative cases;
- two photon resonance and possible odderon production. The contributions of these processes were estimated analytically employing results from [35, 36] and found negligible;
- beam–gas/beam–wall interactions, estimated using pilot bunch events.

The detector response for all generated events is simulated in detail by a program based on GEANT [37]. The simulated events are subject to the same reconstruction procedure as the data.

5 Data Analysis

The measurement is performed on 9.25 pb^{-1} of e^+p data with the centre-of-mass energy $\sqrt{s}$ = 301 GeV, which were collected with the H1 detector at HERA in 1997. For the event selection the following requirements are imposed:

- General selection criteria for the QED Compton process
  - Energies E_1, E_2 of the highest and the second highest energy cluster in the electromagnetic SpaCal
$$E_2 > 4\,\mathrm{GeV}\,, \qquad 20\,\mathrm{GeV} < E_1 + E_2 < 31\,\mathrm{GeV}\,, \tag{3}$$
  - $e\gamma$ acoplanarity
$$A \equiv \pi - \Delta\phi < 45^\circ\,, \tag{4}$$
    where $\Delta\phi$ is the azimuthal angle between the electron and photon directions;
- Additional criteria for inelastic QED Compton process selection
  - At least one cluster with the energy above the noise threshold of 0.5 GeV is found in the LAr calorimeter;
  - $e\gamma$ acoplanarity
$$A > 2^\circ \tag{5}$$
    which suppresses the contamination of elastic QEDC events remaining due to the noise in the LAr calorimeter;
- Background suppression requirements
  - Maximum polar angle of LAr clusters with the energy above the noise threshold
$$\theta_{\mathrm{LAr}} < 30^\circ\,, \tag{6}$$
    which restricts the phase space to the range where the inclusive DIS background is relatively low, and also where the trigger efficiency is high;

– Residual energy in the electromagnetic SpaCal

$$E_{\mathrm{res}} < 1\,\mathrm{GeV} \tag{7}$$

defined as $E_{\mathrm{res}} = E_{\mathrm{tot}} - E_1 - E_2$, where E_{tot} is the total energy in the electromagnetic SpaCal. This cut suppresses DIS, γp, dilepton and vector meson backgrounds;

– Cuts on the lateral shower profiles of the two SpaCal clusters, allowing a good separation of electrons and photons from hadrons;

– Selection of events with the identified electron and photon. The electron identification in BST and CIP involves also the vertex reconstruction;

- Acceptance limits

  – Vertex z coordinate

  $$-30\,\mathrm{cm} < z_{\mathrm{vtx}} < 30\,\mathrm{cm}\,, \tag{8}$$

  which also reduces the beam induced background,

  – Fiducial cuts on the BST and CIP acceptance.

For the kinematic range in question, the reconstruction of the variables x and y cannot be performed using only the four-momenta of the outgoing electron and photon, as the resolution deteriorates with $1/y$ thus becoming inapplicable at low values of the inelasticity y. Therefore these variables have to be reconstructed using in addition the kinematics of the final state hadrons. This is done using the Sigma method [38], which is based on the measurement of $\sum_i (E - p_z)_i$ summing over all objects i of the hadronic final state. Hence one of the main challenges for the analysis is a good understanding of the hadronic final state and the acceptance corrections in this region. The quality of the description employed in the measurement, combining both the hadron distribution by the SOPHIA package and the subsequent simulation of the H1 detector, is illustrated in fig. 2, in which the ratio of the total transverse momentum of measured hadrons $p_{t,\mathrm{had}}$ to the total transverse momentum of the $e\gamma$ system $p_{t,e\gamma}$ is plotted. A very good agreement between data and the simulation is visible[2]. Due to losses in the very forward region, beyond the edge of the LAr calorimeter, the distribution peaks at values smaller than one. One should note, however, that for the calculation of kinematic variables y and x with the Sigma method the total $E - p_z$ of hadrons is used which is much less sensitive to the losses in the beam pipe than the transverse momentum. The acceptance limit defining the lowest measurable y is given by the struck quark direction and is approximately the same as used in inclusive DIS measurements performed by H1.

The control distribution of y shown in fig. 3 demonstrates the good quality of both the hadronic simulation and the cross section description given by the COMPTON program down to the lowest y values, even beyond the range used for the measurement.

The distributions depicted in fig. 4 illustrate a good description of the electron–photon final state provided by the simulation. This was studied additionally with higher precision using all (elastic and inelastic) QED Compton events as shown in fig. 5. For these plots, all analysis cuts except for inelastic QEDC selection, are imposed, thus obtaining an event sample with higher statistics and almost insensitive to hadronisation effects[3].

[2] The peaks in the background distributions are artefacts of the limited MC statistics available at the moment for the inclusive DIS background estimation.

[3] Only due to the cut $\theta_{\mathrm{LAr}} < 30^\circ$ there is a small influence of hadronisation corrections on this event sample.

6 Measurement Uncertainties

The following systematic errors are estimated:

- A 10% uncertainty on the energy attributed to noise or backscattered particles in the LAr calorimeter is estimated studying the energy of the particles rejected by the noise cut. It contributes typically a $4-6\%$ error to the F_2 measurement;
- The uncertainty of the hadronic measurement, which takes into account the errors of the hadronic final state simulation, detector acceptance and LAr calorimeter energy scale, is estimated from the p_t balance between the reconstructed hadron and electron-photon final states. The systematic error is of the order $1-2\%$ rising up to 6% at lowest y values;
- The uncertainty of the SpaCal energy scale, affecting simultaneously the energies of both clusters, amounts to 1% at $E > 17\,\mathrm{GeV}$ and increases linearly at lower energies up to 2.7% at $E = 4\,\mathrm{GeV}$. This source contributes $1-2\%$ error to the measurement;
- The uncertainties of the measurement due to polar angle and z_{vtx} reconstruction are typically within 1%;
- The total efficiency of the electron/photon identification and vertex reconstruction is studied using inclusive DIS and elastic QEDC events and the corresponding error of the measurement is estimated to be 3%;
- Out of the errors of the background estimation, as described in sect. 4, main contributions are 5.5% by inelastic DVCS and up to 3% by inclusive DIS. Other errors are below 1%;
- The luminosity measurement contributes a 1.5% error;
- The uncertainties of several trigger conditions stay each within 0.5%;
- The error due to radiative corrections amounts to 2%.

Both the statistical and the systematic errors lie in the range $8-13\%$ making thus the total error to be $12-18\%$.

7 Results of the Measurement

In order to extract the structure function F_2 the data sample is divided into subsamples corresponding to a grid in y and Q^2. The bin sizes are adapted to the resolution in the measured kinematic quantities such that purity and stability in all bins shown are greater than 30%. Here, the purity (stability) is defined as the ratio of the number of simulated QEDC events originating from and reconstructed in a specific bin to the number of reconstructed (generated) events in the same bin.

The F_2 values measured in QED Compton scattering are depicted in fig. 6 as a function of x at fixed Q^2 and compared to other HERA [7, 39, 40] and fixed target [41–43] data. The present analysis extends the kinematic range of HERA at very low Q^2 towards higher x values thus complementing standard inclusive and shifted vertex measurements. For inclusive DIS at nominal vertex position the outgoing electron is not detected in the H1 apparatus for such low values of Q^2 as it is scattered at small angles escaping through the beam pipe unseen. On the other hand shifted vertex data cannot extend the low Q^2 measurements to such high x due to stronger acceptance limitations in the forward region. The region covered mostly overlaps with the domain of fixed target experimets. A good agreement with their results is observed.

8 Summary

Preliminary results of a measurement of the proton structure function F_2 in QED Compton scattering at HERA are presented. The data analysis is performed at very low Q^2 down to $0.1\,\mathrm{GeV}^2$, in the transition region from DIS to photoproduction. The measurement extends the kinematic domain of HERA complementing the analyses of standard inclusive low Q^2 and shifted vertex data in the medium x region. The results are in a good agreement with data of fixed target experiments.

References

[1] D. J. Fox *et al.*: Phys. Rev. Lett. **33** (1974) 1504.

[2] J. G. de Groot *et al.*: Z. Phys. C **1** (1979) 143.

[3] C. Adloff *et al.* [H1 Collaboration]: Eur. Phys. J. C **21** (2001) 33 [hep–ex/0012053].

[4] S. Aid *et al.* [H1 Collaboration]: Nucl. Phys. B **470** (1996) 3 [hep–ex/9603004].

[5] M. Derrick *et al.* [ZEUS Collaboration]: Z. Phys. C **72** (1996) 399 [hep–ex/9607002].

[6] C. Adloff *et al.* [H1 Collaboration]: Phys. Lett. B **393** (1997) 452 [hep–ex/9611017].

[7] J. Breitweg *et al.* [ZEUS Collaboration]: Phys. Lett. B **487** (2000) 53 [hep–ex/0005018].

[8] P. D. Collins: **An Introduction To Regge Theory And High-Energy Physics**, Cambridge, 1977, 445p.

[9] M. Derrick *et al.* [ZEUS Collaboration]: Z. Phys. C **69** (1996) 607 [hep–ex/9510009].

[10] C. Adloff *et al.* [H1 Collaboration]: Nucl. Phys. B **497** (1997) 3 [hep–ex/9703012].

[11] A. Courau and P. Kessler: Phys. Rev. D **46** (1992) 117.

[12] T. Ahmed *et al.* [H1 Collaboration]: Z. Phys. C **66** (1995) 529.

[13] T. Carli, A. Courau, S. Kermiche and P. Kessler: in **Proceedings of the Workshop "Physics at HERA", Hamburg, 1991**, DESY, 1992, Vol. 2, p. 902 and Vol. 3, p. 1468.

[14] E. Etim, G. Pancheri and B. Touschek: Nuovo Cim. B **51S10** (1967) 276.

[15] G. Pancheri: Nuovo Cim. B **60S10** (1969) 321.

[16] V. Lendermann: Doctoral Thesis, University of Dortmund, 2002.

[17] F. W. Brasse *et al.*: Nucl. Phys. B **110** (1976) 413.

[18] H. Abramowicz and A. Levy: hep–ph/9712415.

[19] A. Mücke *et al.*: Comput. Phys. Commun. **124** (2000) 290 [astro–ph/9903478].

[20] T. Sjöstrand *et al.*: Comput. Phys. Commun. **135** (2001) 238.

[21] A. Capella, U. Sukhatme, C. Tan and J. Tran Thanh Van:
Phys. Rept. **236**, 225 (1994).

[22] I. Abt *et al.* [H1 Collaboration]: Nucl. Instrum. Meth. A **386** (1997) 310 and 348.

[23] R. D. Appuhn *et al.* [H1 SpaCal Group]:
Nucl. Instrum. Meth. A **374** (1996) 149, A **382** (1996) 395 and A **386** (1997) 397.

[24] B. Schwab: Doctoral Thesis, Ruprecht Karl University of Heidelberg, 1996.

[25] V. Arkadov: Doctoral Thesis, Humboldt University of Berlin, 2000.

[26] G. A. Schuler and H. Spiesberger: in **Proceedings of the Workshop "Physics at HERA", Hamburg, 1991**, DESY, 1992, Vol. 3, p. 1419.

[27] R. Ingelman: in **Proceedings of the Workshop "Physics at HERA", Hamburg, 1991**, DESY, 1992, Vol. 3, p. 1366.

[28] L. Lönnblad: Comput. Phys. Commun. **71** (1992) 15.

[29] A. Kwiatkowski, H. Spiesberger and H. J. Mohring: Comput. Phys. Commun. **69** (1992) 155. Also in **Proceedings of the Workshop "Physics at HERA", Hamburg, 1991**, DESY, 1992, Vol. 3, p. 1294.

[30] R. Stamen: Doctoral Thesis, University of Dortmund, 2001.

[31] C. Adloff *et al.* [H1 Collaboration]: Phys. Lett. B **517** (2001) 47 [[hep–ex/0107005].

[32] T. Abe *et al.*: in **Proceedings of the Workshop "Monte Carlo Generators for HERA Physics", Hamburg 1998–1999**, p. 566.

[33] R. Engel and J. Ranft: Phys. Rev. D **54** (1996) 4244, [hep–ph/9509373].

[34] B. List, A. Mastroberardino: in **Proceedings of the Workshop "Monte Carlo Generators for HERA Physics", Hamburg 1998–1999**, p. 396.

[35] W. Kilian and O. Nachtmann: Eur. Phys. J. C **5** (1998) 317 [hep–ph/9712371].

[36] E. R. Berger *et al.*: Eur. Phys. J. C **9** (1999) 491 [hep–ph/9901376].

[37] R. Brun *et al.* [GEANT Team]: CERN Program Library Long Writeup W5013.

[38] U. Bassler and G. Bernardi: Nucl. Instrum. Meth. A **361** (1995) 197 [hep–ex/9412004].

[39] H1 Collaboration: contributed paper to the International Europhysics Conference on High Energy Physics, EPS 2001, Budapest; Abstract **799**, Parallel Session **1**.

[40] H1 Collaboration: contributed paper to the International Europhysics Conference on High Energy Physics, EPS 2003, Aachen; Abstract **082**, Parallel Session **4**.

[41] L. W. Whitlow *et al.*: Phys. Lett. B **282** (1992) 475.

[42] M. Arneodo *et al.* [New Muon Collaboration], Nucl. Phys. B **483** (1997) 3 [hep–ph/9610231].

[43] M. R. Adams *et al.* [E665 Collaboration]: Phys. Rev. D **54** (1996) 3006.

[44] T. Laštovička, Eur. Phys. J. C **24** (2002) 529 [hep–ph/0203260].

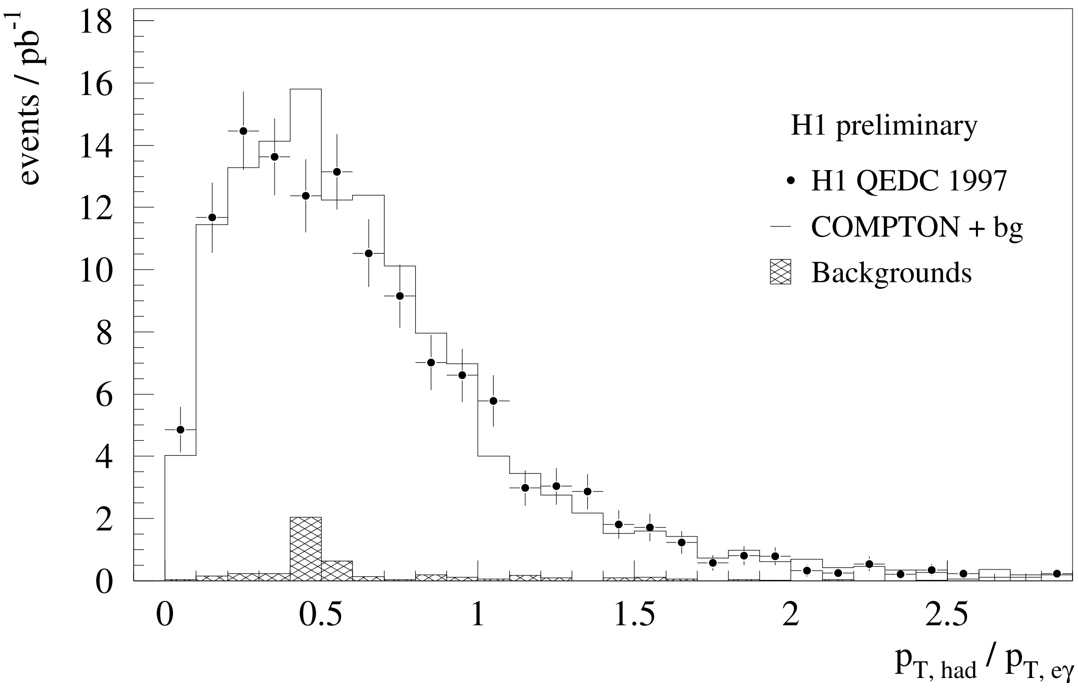

Figure 2: Ratio of the total measured transverse momentum of hadrons to the total transverse momentum of the $e\gamma$ system. H1 data are depicted by the closed circles. The solid histogram represents the sum of COMPTON MC events with all background contributions added. The hatched histogram denotes the sum of all simulated background events

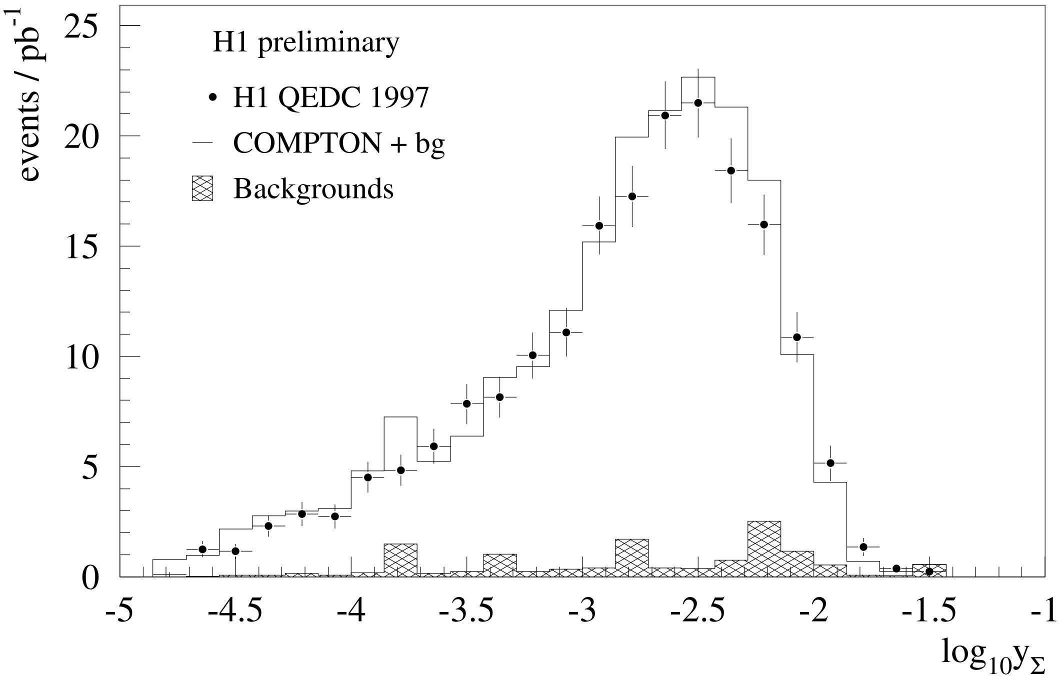

Figure 3: y_Σ distribution after applying all selection cuts. The solid histogram represents the sum of COMPTON MC events with all background contributions added. The hatched histogram denotes the sum of all simulated background events

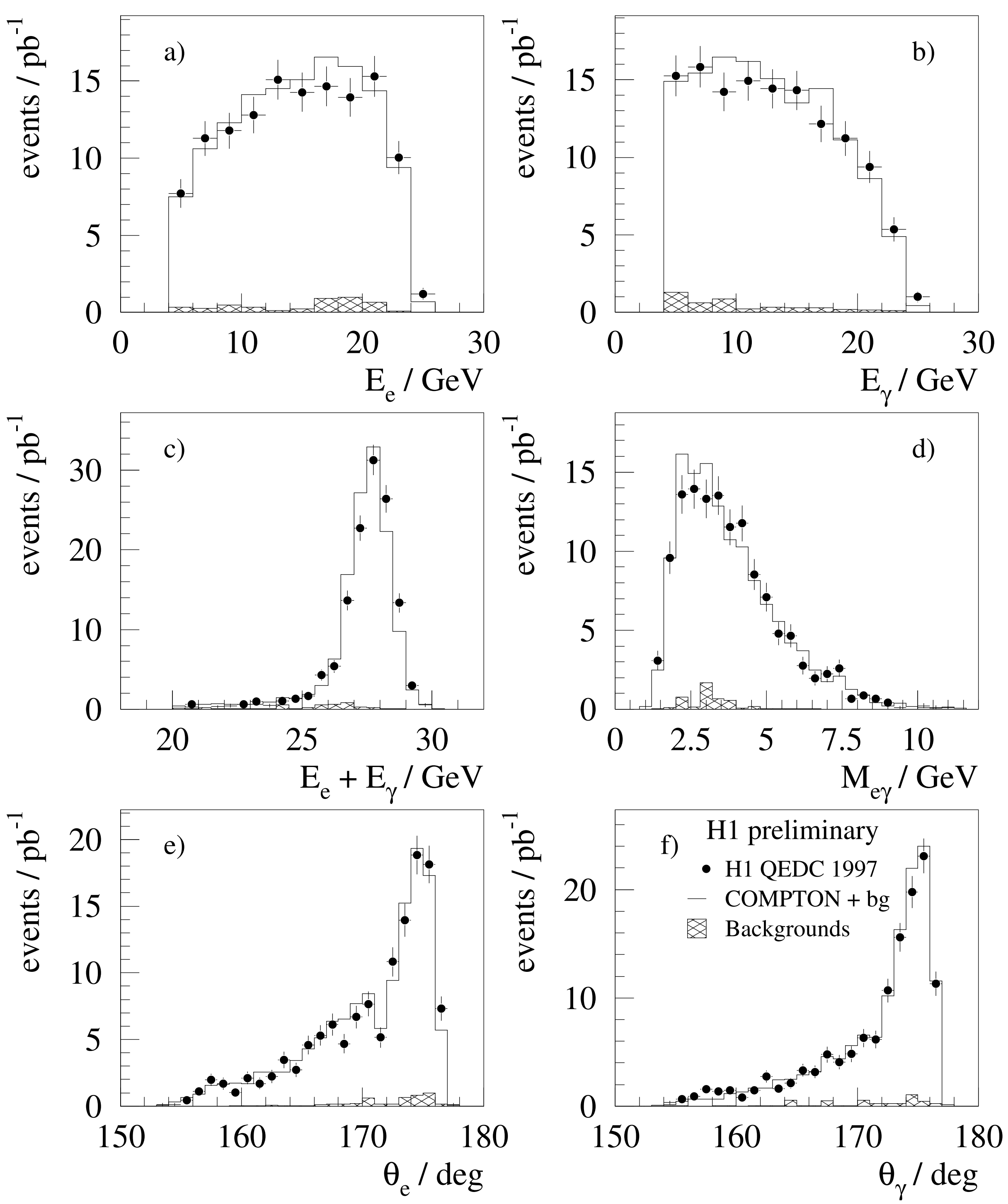

Figure 4: Control distributions for the measured electron and photon in events used for the measurement. Shown are: a) electron energy, b) photon energy, c) sum of both energies, d) invariant mass of the $e\gamma$ system, e) electron scattering angle and f) photon scattering angle

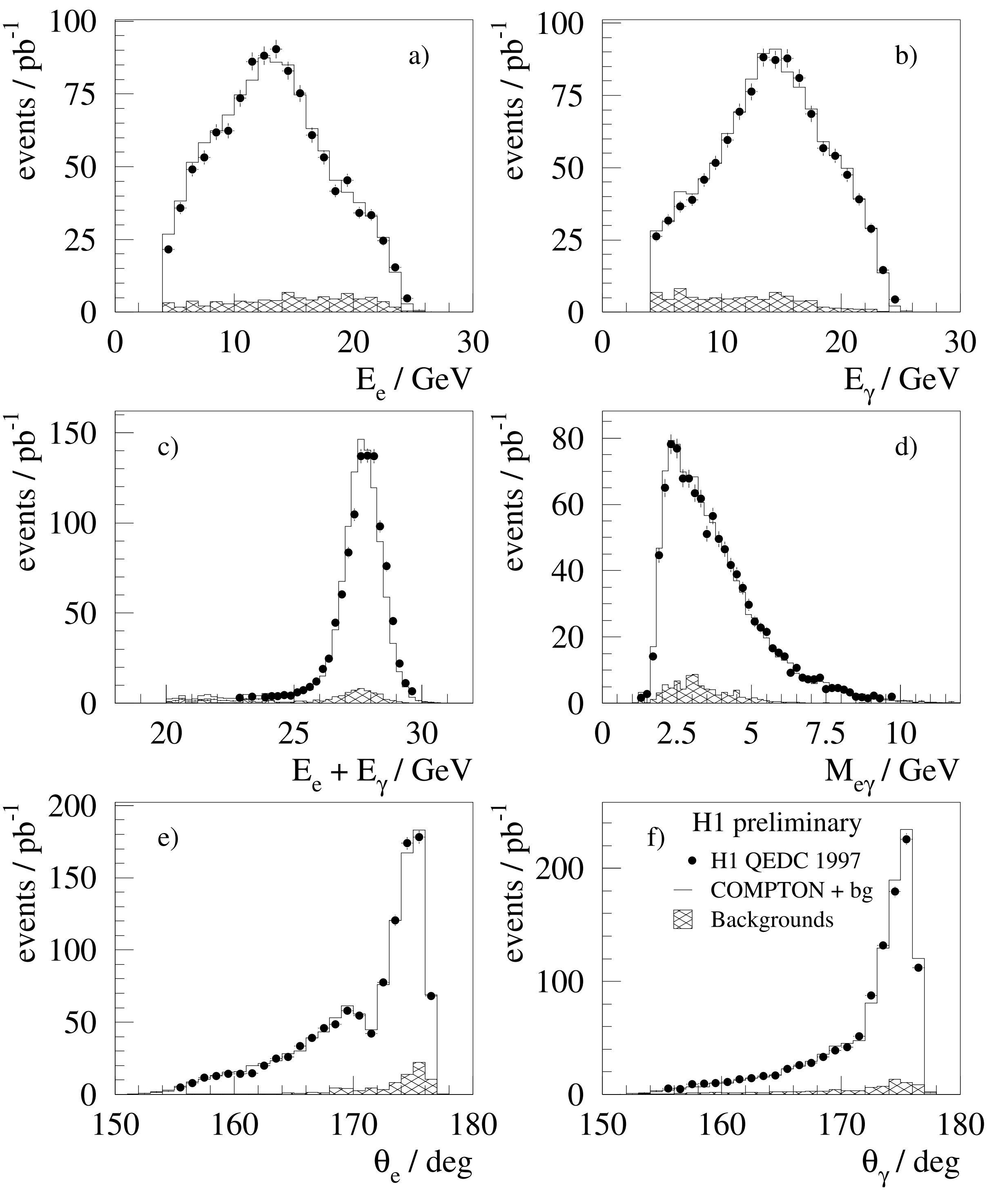

Figure 5: Control distributions for the measured electron and photon in all (elastic and inelastic) QED Compton events. All selection cuts are applied except those demanding explicitly inelastic events. Shown are: a) electron energy, b) photon energy, c) sum of both energies, d) invariant mass of the $e\gamma$ system, e) electron scattering angle and f) photon scattering angle

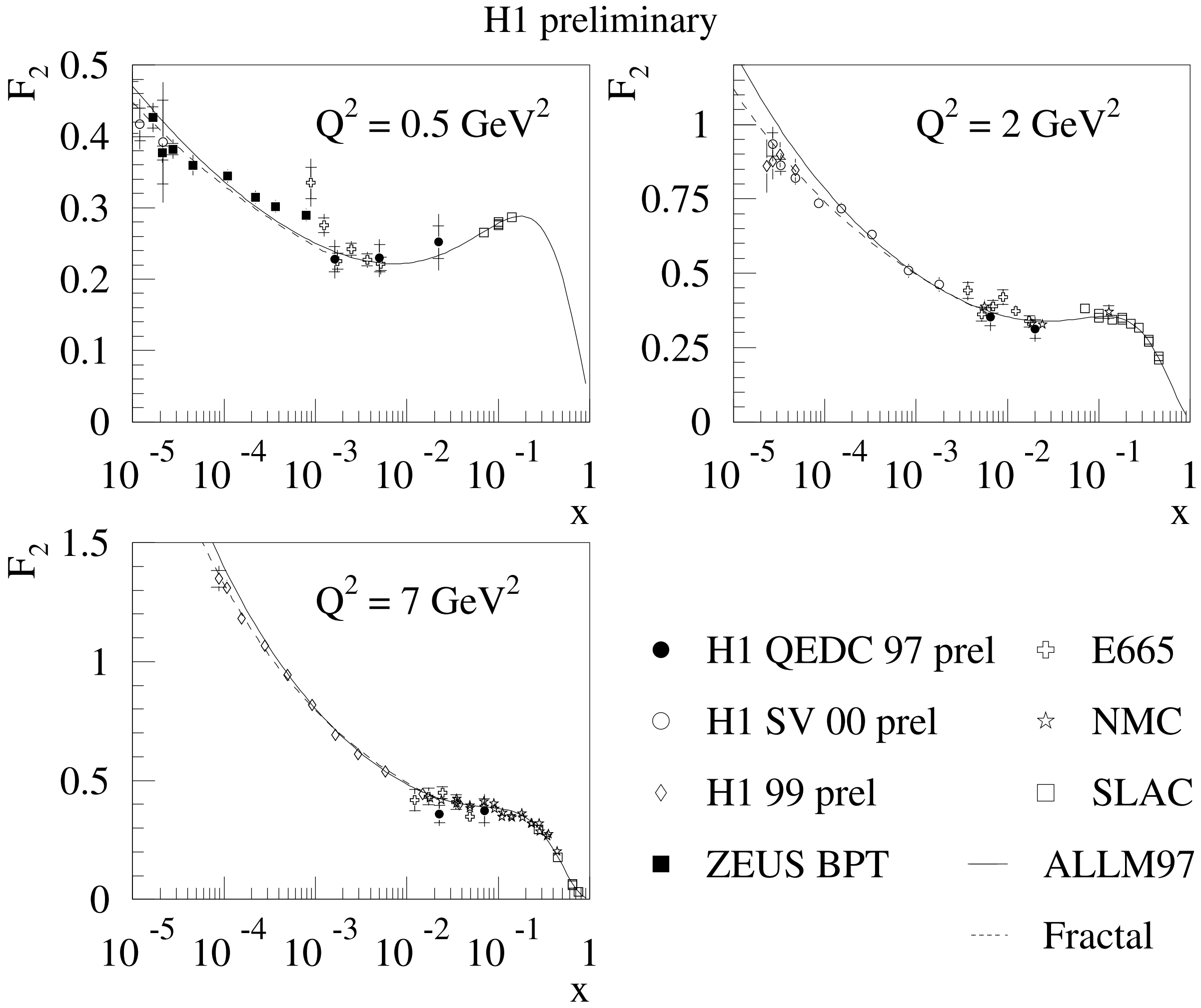

Figure 6: Results of F_2 measurement in QED Compton scattering (closed circles) compared with other measurements at HERA (closed squares [7], open diamonds [39] and open circles [40]) and fixed target experiments (open squares [41], open stars [42] and open crosses [43]). The solid line depicts the ALLM97 parameterisation [18], while the dashed line represents the Fractal fit [44], which is plotted in the range $y > 0.003$.